Results of the Cycle 4 FOC DQE Program

R. Jedrzejewski
January 15, 1996

ABSTRACT

This report describes the calibration of the FOC+COSTAR DQE from in-orbit data. Two spectrophotometric standard stars were observed through many FOC filters to determine the absolute sensitivity. The data were analyzed in a significantly different fashion from earlier (pre-COSTAR) data, largely because of the smaller field of view of the COSTAR-corrected FOC. It was found that the (Observed/Expected) fluxes followed a linear relation with wavelength, and when the FOC DQE curve was corrected by this function, r.m.s. residual errors of only 6% in the absolute flux determination remained. Analysis of the ND filter transmissions did not show any significant differences between the observed and expected throughputs, although more work is needed to check this finding. The Pseudo-Strehl and FWHM performance characteristics of the FOC were measured and plotted to assist potential users, and a comparison of FOC and WFPC2 sensitivities in the ultraviolet shows that the FOC is significantly more sensitive for all wavelengths below 4000Å.

1. Introduction

The measurement of the Detective Quantum Efficiency (DQE) for the FOC is essential since all absolute flux estimation relies on accurate calibration of this quantity. This can be accomplished by observing spectrophotometric standard stars whose absolute fluxes are known from IUE measurements in the ultraviolet and, often, scanner measurements in the visible. This report describes the results of a program to measure the FOC DQE.

2. History

The throughput curves that are used to calculate the FOC inverse sensitivities have several components; the OTA transmission (which includes the reflectivity of the OTA mirror surfaces and the central obstruction), the COSTAR reflectivities (after the First Servicing Mission), the FOC sensitivity and the FOC filter throughputs. The FOC DQE file in use until October 1994 (FOC_96_DQE_003) was derived from SV calibration measurements of spectrophotometric standard stars (see FOC Instrument Science Report FOC-053).

After the First Servicing Mission, the effect of COSTAR was represented by introducing the COSTAR throughput curve (FOC_96_M1M2_001), which was derived from ground measurements of the reflectivities of witness mirrors measured at GSFC shortly after they were coated. Preliminary measurements of the reflectance of the COSTAR mirrors using in-orbit measurements of a standard star just before and after COSTAR deployment showed that the COSTAR reflectivity curve in the CDBS was correct to within the observational errors (5-10%). This Report describes measurement of the overall sensitivity of the OTA+COSTAR+FOC system using filtered measurements of spectrophotometric standard stars.

3. Observations, data reduction

Observations of spectrophotometric standard stars taken after the installation of COSTAR were included. These came from 3 programs:

SMOV/4787 “FOC/COSTAR Absolute Sensitivity”

SMOV/4788 “FOC/COSTAR Point-Spread Function”

CAL/5517 “FOC Absolute Sensitivity - Cycle 4”

The first two of these programs were SMOV programs executed just after the alignment of the COSTAR/FOC mirrors, while the third program was executed approximately 2 1/2 months later as part of the Cycle 4 FOC calibration plan. A wide assortment of filters was used on two different targets; details are in Table 1. The filters were chosen to cover a wide range of central wavelengths and to cover most or all of the filters that were to be used by GOs and GTOs in Cycle 4. Most of the observations required the use of neutral density filters to bring the count rate into the linear regime for the FOC, more on this in a later section.

Table 1. Summary of the Observations

Rootname	Format	Filters	Target	Exposure Time (s)	Predicted Rate (c/s)
x23k0102t	512x512	F140M+F2ND	BPM	896.0	43.973
x23k0103t	512x512	F170M+F4ND	BPM	896.0	7.975
x23k0104t	512x512	F210M+F4ND	BPM	896.0	11.894
x23k0105t	512x512	F307M+F4ND	BPM	896.0	45.030
x23k0106t	512x512	F410M+F4ND	BPM	896.0	26.985
x23k0107t	512x512	F501N+F1ND	BPM	896.0	34.706
x23k0108t	512x512	F550M+F1ND	BPM	896.0	41.635
x2340102t	256x256	F120M	BPM	895.875	50.479
x2340103t	256x256	F152M+F2ND	BPM	895.875	56.679
x2340104t	256x256	F220W+F4ND+F1ND	BPM	895.875	31.057
x2340105t	256x256	F342W+F6ND	BPM	895.875	29.296

Rootname	Format	Filters	Target	Exposure Time (s)	Predicted Rate (c/s)
x2340106t	256x256	F372M+F4ND+F1ND	BPM	895.875	38.125
x2340107t	256x256	F430W+F4ND+F1ND	BPM	895.875	62.656
x2340108t	256x256	F486N	BPM	895.875	47.470
x2340109t	256x256	F480LP+F2ND+F1ND	BPM	895.875	74.510
x234010at	256x256	F501N+F1ND	BPM	895.875	41.647
x2ap0102t	512x512	F210M+F4ND	HZ4	595.875	5.542
x2ap0104t	256x256	F210M+F4ND	HZ4	285.875	6.651
x2ap0105t	256x256	F210M+F4ND	HZ4	305.875	6.651
x2ap0106t	256x256	F210M+F2ND	HZ4	295.875	54.449
x2ap0107t	256x256	F210M+F2ND	HZ4	295.875	54.449
x2ap010bt	256x256	F120M	HZ4	715.875	7.848
x2ap010ct	256x256	F152M	HZ4	355.875	107.870
x2ap010dt	256x256	F165W+F4ND	HZ4	455.875	28.374
x2ap010et	256x256	F140W+F2ND	HZ4	295.875	63.019
x2ap010ft	256x256	F175W+F2ND+F1ND	HZ4	295.875	64.588
x2ap010gt	256x256	F190M+F2ND	HZ4	335.875	42.100
x2ap010ht	256x256	F190M+F2ND	HZ4	187.875	42.100
x2ap010it	256x256	F195W+F4ND	HZ4	355.875	59.906
x2ap010jt	256x256	F220W+F4ND	HZ4	595.875	37.273
x2ap010kt	256x256	F275W+F4ND	HZ4	395.875	71.961
x2ap010lt	256x256	F278M+F2ND+F1ND	HZ4	295.875	70.022
x2ap0202t	256x256	F342W+F4ND+F1ND	HZ4	355.875	54.736
x2ap0203t	256x256	F372M+F4ND	HZ4	355.875	65.616
x2ap0204t	256x256	F346M+F4ND	HZ4	355.875	60.070
x2ap0205t	256x256	F480LP+F2ND+F1ND	HZ4	295.875	63.651
x2ap0206t	256x256	F410M+F2ND+F1ND	HZ4	295.875	47.326
x2ap0207t	256x256	F430W+F4ND+F1ND	HZ4	495.875	44.763
x2ap0208t	256x256	F502M+F2ND+F1ND	HZ4	257.875	40.914
x2ap0209t	256x256	F502M+F2ND+F1ND	HZ4	233.875	40.914
x2ap020at	256x256	F550M+F1ND	HZ4	495.875	44.456
x2ap020bt	256x256	F501N+F1ND	HZ4	495.875	35.545
x2ap020ct	256x256	F501N	HZ4	351.875	108.464
x2ap020dt	256x256	F501N+F2ND	HZ4	295.875	17.802

Measurement of the quantum efficiency of the FOC requires determining the total count rate from a star whose absolute flux is accurately known. The total count rates were calculated using a program COSTAREE, originally written in FORTRAN but re-coded into SPP so that it would be more portable.

The total count rate is actually unmeasurable, since the light from a point source is imaged into a distribution that is not fully contained in a finite aperture size. Without knowing the

flux distribution in the PSF, one cannot extrapolate from the measured flux within a finite aperture size to the extrapolated 'total' flux. The best that one can do is to specify an aperture size within which the flux is measured, and then DEFINE the DQE as the ratio of measured flux within the designated aperture to the total flux incident from the standard star. This is the approach that was adopted for measurement of the DQE in Science Verification (see Instrument Science Report FOC-053); an aperture radius of 3.0 arcsec was used.

An added complication comes from the fact that the measured flux contains background counts in addition to the counts from the standard star. Again, to measure the background count rate one must attempt to measure the flux at a distance sufficiently far from the star that the stellar contribution can be considered negligible. This was done in SV; the sky was determined between 150 and 175 pixels radius (3.345-3.903 arcsec radius).

Alternatively, one can DEFINE the background as the value that is measured at a particular distance from the star, or else as the value that causes the encircled energy curve to behave in a way that mimics what would be seen if the all of the flux from the star were contained within the chosen aperture. The latter approach is used here.

If all of the flux is contained within a given aperture size, then the intensity from the star will, by definition, fall to zero at the boundary of the aperture. This will also make the encircled energy curve asymptotically approach a limit at the edge of the aperture. If one were to investigate the behavior of the profile and encircled energy curve outside the chosen aperture, one would see that the profile would become ***negative*** and the encircled energy curve would ***fall***. This is of course not the behavior one would like, but in practice, perhaps one does not have access to the image outside the chosen aperture size, or else one can legitimately consider counts that fall outside this aperture as 'useless' for astronomical purposes.

For this study, the aperture size was chosen to be a circle of radius 70 pixels. Using the best estimate of the plate scale, this is equivalent to 1.0045 ± 0.001 arcsec. For all practical purposes, this can be considered as 1.000 arcsec.

The algorithm used to calculate the azimuthally-averaged PSF profile and encircled energy curve is very simple. The brightest pixel in the PSF is defined as the PSF center. Then each pixel in the image is assigned an integer radial coordinate by simply measuring the distance from the adopted PSF center. Array elements corresponding to this integer are incremented by the counts in that pixel and 1 respectively, which corresponds to specifying an annulus within which the counts in that pixel fall. After each pixel has been so analyzed, the mean intensity for each annulus is calculated as the total counts divided by the number of pixels within the annulus.

The encircled energy is calculated as the total counts within circles of increasing radii, or simply as the cumulative sum of counts within the annuli described in the previous para-

graph. A radial coordinate is calculated for each ‘circle’ as the radius of the circle that has the same area as the (approximately circular) shape defined by all the pixels that are closer than a specified distance from the PSF center.

The background is determined as that value which makes that encircled energy curve ‘flat’ over the radial distance between 63 and 77 pixels (0.9041” and 1.1050”). Specifically, the value is chosen that minimizes the r.m.s. scatter of the 14 encircled energy measurements in that radial range. For a given background value, the encircled energy values are re-calculated as the total enclosed flux values minus the background multiplied by the number of enclosed pixels.

This definition of background has the desirable property of making the encircled energy curve appear to asymptotically approach a limit at 1 arcsecond radius. To all intents and purposes, the flux outside 1 arcsecond does not contribute to the DQE measurement.

The **stsdas** task **synphot** is used to predict the count rate from a star whose spectrum is known by folding the spectrum through the various HST sensitivity curves. For the COSTAR-corrected FOC, these curves are the HST OTA throughput, the COSTAR mirrors’ throughput, the FOC quantum efficiency and the FOC filter transmission curves. Thus, the flux in erg cm^{-2} s^{-1} $Å^{-1}$ from the star is converted to a predicted flux in detected photons s^{-1} at the detector. A discrepancy between the predicted value with the actual value measured indicates that one of the throughput curves used to make the prediction is incorrect.

For this exercise, we can assume that the OTA throughput and collecting area are known. The COSTAR mirrors’ throughputs were measured soon after coating and then again about 6 months later. In principle, the latter COSTAR transmission curves are applicable, but they are only specified at a relatively small number of wavelengths. For the purposes of this study, where the effective total system throughput of the OTA+COSTAR+FOC/96 chain is desired, it doesn’t matter whether we consider the discrepancies between observed and predicted count rates as due to incorrectly specified COSTAR throughputs or FOC DQE curves, the net effect is the same. We chose to keep the COSTAR reflectivities the same and modify the FOC DQE curve.

Measurements of BPM16274 just before COSTAR installation and just after alignment indicated that, to the accuracy of the observations, the COSTAR throughput is consistent with that measured on the ground, so keeping the COSTAR throughput at the ground measured values is a reasonable thing to do.

4. Results

The results of the analysis are presented in Table 2. The observed/expected ratio is calculated for each filter combination. By plotting this ratio as a function of wavelength, it is possible to determine how to correct the FOC DQE file. However, it is not entirely obvious what one should use for the ‘wavelength’ of a particular observation, since the detected

photons form a distribution over wavelength. For this study the wavelength was calculated by forming the cumulative distribution of detected photons, and calculating the mean wavelength of detected photons between the 25th and 75th percentiles. The choice of algorithm for calculating the effective wavelength is not critical.

Table 2. Results of the DQE Analysis

Rootname	Background (counts/pix)	Measured count rate (counts/sec)	Effective Wavelength	Ratio (Observed/ Expected)
x23k0102t	0.6571	31.797	1456.1	0.759
x23k0103t	0.5193	5.903	1799.7	0.788
x23k0104t	0.6041	7.956	2159.8	0.720
x23k0105t	0.6179	31.841	3061.0	0.741
x23k0106t	0.6979	26.385	4085.4	1.010
x23k0107t	0.6315	37.554	5018.2	1.113
x23k0108t	0.7634	41.375	5500.7	1.021
x2340102t	1.1369	39.924	1282.0	0.843
x2340103t	1.0234	40.846	1531.5	0.758
x2340104t	0.7926	25.069	2304.3	0.862
x2340105t	0.9783	28.666	3351.3	1.021
x2340106t	0.8306	40.215	3688.4	1.096
x2340107t	1.3819	69.638	4083.6	1.149
x2340108t	0.8770	46.989	4867.4	1.018
x2340109t	1.1900	89.338	5172.6	1.232
x234010at	0.9243	51.167	5018.2	1.263
x2ap0102t	0.4038	3.688	2163.4	0.716
x2ap0104t	0.2152	4.719	2163.4	0.764
x2ap0105t	0.2215	4.338	2163.4	0.702
x2ap0106t	0.1997	37.621	2158.4	0.744
x2ap0107t	0.2454	37.763	2158.4	0.747
x2ap010bt	0.8434	4.457	1461.1	0.599
x2ap010ct	0.4192	81.306	1548.3	0.793
x2ap010dt	0.3788	22.887	1905.6	0.857
x2ap010et	0.2445	51.755	1521.3	0.864
x2ap010ft	0.2539	52.036	1828.6	0.857
x2ap010gt	0.4733	36.281	2002.4	0.927
x2ap010ht	0.2448	35.736	2002.4	0.913
x2ap010it	0.3080	51.408	2169.6	0.911
x2ap010jt	0.4069	31.644	2306.7	0.907
x2ap010kt	0.4572	59.621	2771.6	0.872
x2ap010lt	0.3119	59.233	2800.0	0.890
x2ap0202t	0.2625	53.715	3367.3	1.024
x2ap0203t	0.2773	63.074	3701.0	0.998
x2ap0204t	0.4702	57.626	3462.2	1.000
x2ap0205t	0.2441	67.164	5187.3	1.085
x2ap0206t	0.2452	47.220	4084.3	1.031
x2ap0207t	0.3989	41.815	4107.7	0.965
x2ap0208t	0.2968	40.371	4981.7	1.015
x2ap0209t	0.2614	40.459	4981.7	1.017
x2ap020at	0.3413	47.954	5500.7	1.108

Rootname	Background (counts/pix)	Measured count rate (counts/sec)	Effective Wavelength	Ratio (Observed/ Expected)
x2ap020bt	0.3605	37.874	5018.7	1.096
x2ap020ct	0.4018	107.487	5018.7	1.019
x2ap020dt	0.2023	13.278	5018.7	0.767

The results of the analysis are presented in Figure 1.

Figure 1: Results of the DQE analysis. The solid line is the best-fit straight line. The dispersion around this fit is 0.094. All of the data points from Table 2 are plotted.

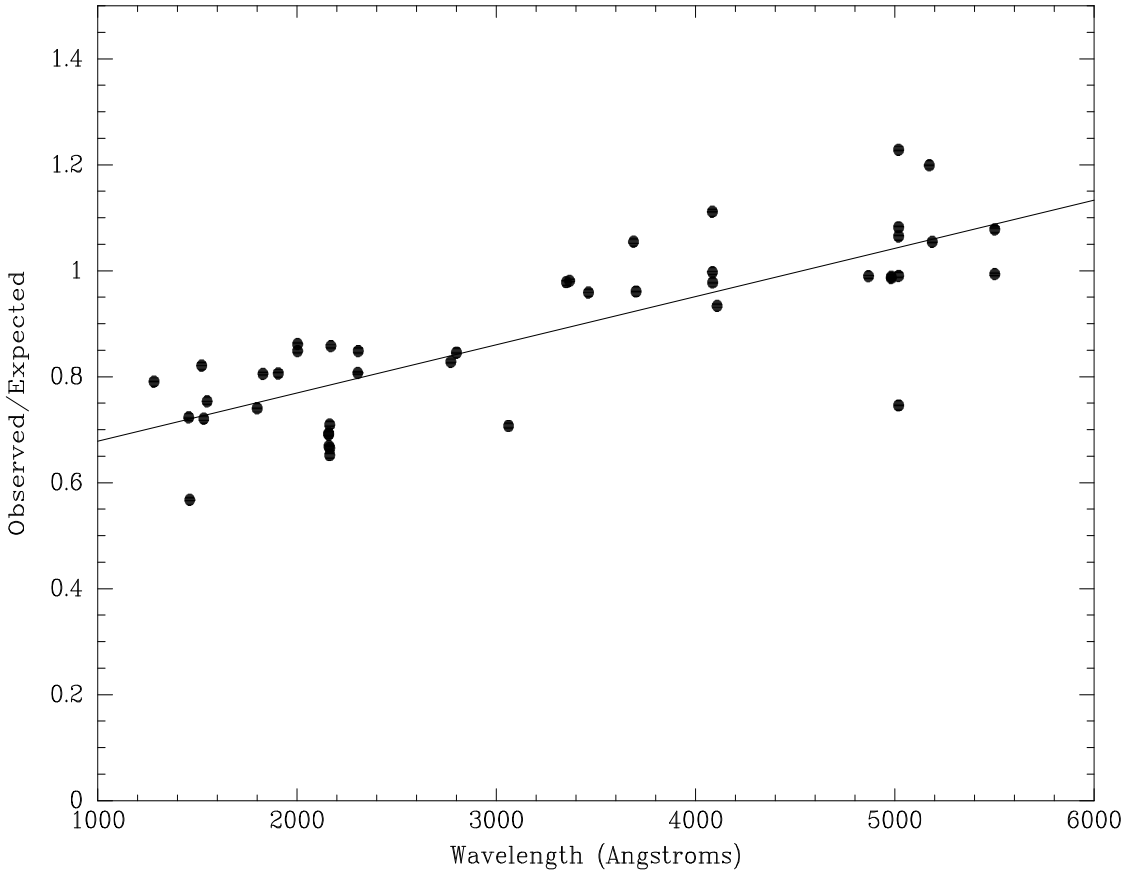

The points show a roughly linear relation between (Observed/Expected) flux and effective wavelength, with an r.m.s deviation around the best fit straight line of 0.094. It was not considered worthwhile to try to fit a higher-order function, since the dispersion within small wavelength ranges was a significant fraction of the r.m.s.

There are several reasons why the run of (Observed/Expected) with wavelength is not a horizontal line with value 1.0:

Light between 1 arcsec and 3 arcsec

Because of the smaller pixels of the COSTAR-corrected FOC (0.01435” vs. 0.0223”) and the fact that most of the observations were made using the 256x256 format, it was clearly not possible to use the same algorithm for calculating the encircled energy as was used in SV. The use of a smaller aperture (1” instead of 3”) means that the light from the PSF that falls between 1” and 3” is now not counted towards the total flux from the star. The amount of light in the range 1-3” can be measured by analyzing the BPM16274 data taken with the 512x512 format using an algorithm similar to that used to analyze the SV data. It was found that typically the fluxes within 1” were approximately 10-20% lower than those within 3”. Surprisingly, little trend was found with wavelength, so this does not explain the wavelength dependence of the (Observed/Expected) values. However, one must perhaps temper this measurement with recognition that the background was determined from an area close to the edge of the 512x512 format, and so might be subject to greater uncertainty.

Indeed, inspection of the encircled energy curves showed that background unevenness over the field was contributing to somewhat anomalous encircled energy curves. Inspection of all of the encircled energy curves did show a tendency for there to be more flux in the outermost points at short wavelengths than at longer wavelengths, as could be seen by the fact that the curves approached their asymptotic values further in for longer wavelengths. For this reason, the scattered light between 1” and 3” is considered to be the primary contributor to the slope of the (Observed/Expected) line.

Updated spectrophotometry for BPM16274 and HZ4

The spectrophotometry files for the standard stars BPM16274 and HZ4 were corrected using the correction of Bohlin as outlined in ISR CAL-002 (December 1993). This correction makes the predicted fluxes approximately 10% higher in the 1200-2000Å wavelength range and approximately 5% higher in the 2000-2500Å range. Of course this makes the (Observed/Predicted) values correspondingly lower.

Drop in FOC sensitivity from 1990-1993

When the FOC sensitivity was measured by Hodge (ISR FOC-071) and Greenfield (ISR FOC-078) using data from Cycles 2 and 3, it was found to be approximately 3-5% lower than was measured in SV.

COSTAR mirrors aging

The COSTAR reflectivities that are in CDBS were measured just after the mirrors were coated. A subsequent measurement of witness samples approximately 6 months after coating showed approximately 5% of degradation.

Unknown factors

None of the above factors can make the (Observed/Expected) values >1, so the fact that points with $\lambda > 4500$Å appear to be >1 is something of a surprise. Possible explanations involve uncertainty in the HZ4 spectrophotometry and uncertainties in the format-dependent sensitivity.

This means that if we were to correct the overall throughput of the OTA+COSTAR+FOC system using this linear function, the 1σ error on the absolute measurement of the flux of a star would be approximately 10%. This error is made up of the many contributions (flat-fielding, photon statistics, background subtraction, pattern noise, nonlinearity, inaccuracy of filter transmission curve, etc.), but assumes that the absolute fluxes used to calculate the predicted count rates are perfectly correct. While this performance is quite good, it is worthwhile to investigate whether some of the discrepant points might be so for reasons other than those listed. In other words, the data should be weeded to remove observations that we have reason to believe might be giving us the wrong answer. Four classes of suspect observations were considered:

1. visual observations of BPM16274, where the reference spectrum is a model
2. repeated observations over-represented
3. observations with high count rate possibly nonlinear
4. observations with low count rate have higher statistical errors

Visual Observations of BPM16274

The reference spectrum for BPM16274 (crcalspec$bpm16274_001.tab) consists of IUE measurements from 1160-1200Å and 1225-3150Å. Outside of this range, a model DA white dwarf spectrum is used. While the model and observed spectra agree well over the range of overlap, in the visual range the computed UBV magnitudes do not agree well with the UBV magnitudes measured from the ground, with differences of (0.18, 0.16, 0.15) mag in (U, B, V). For this reason, observations of BPM16274 with an effective wavelength longer than 3150 Å were not included. The F307M observation falls below the cutoff, while F342W is above.

Removing the 9 visual-band observations of BPM16274 reduced the r.m.s. from 0.0938 to 0.0848. While this does not sound like much, it corresponds to removing 0.040 in quadrature.

Repeated Observations Over-represented

Some observations are repeated purely to fill orbits more efficiently: for example, the F210M+F4ND observations of HZ4 are split into 285.875 + 305.875s. Combining the two observations gives a total exposure time equivalent to a single 600s exposure (apart from a

small dead time difference). It is more reasonable to use the single combined count rate than two individual measurements, because in the latter case the measurements are given twice the weight of unsplit observations.

Combining the 4 pairs of split observations in this way actually increased the r.m.s. slightly, to 0.0852.

Observations with high & low count rates

For some observations, the count rate might take the data into the non-linear regime. For others, the count rate might be so low that errors in background subtraction can dominate since within the large aperture considered, the total count rate from the background is larger than that from the target. To investigate, the residual from the best straight-line fit were plotted against count rate. The results, shown in Figure 2, show that none of the observations appear to have a high enough count rate to cause nonlinearity problems, but that observations with a low count rate (<20.0 counts/sec) have a higher dispersion. For this reason, the six points from observations with a rate < 20.0 counts/sec were removed from the sample.

Figure 2: Plot of residual from best straight-line fit against measured count rate.

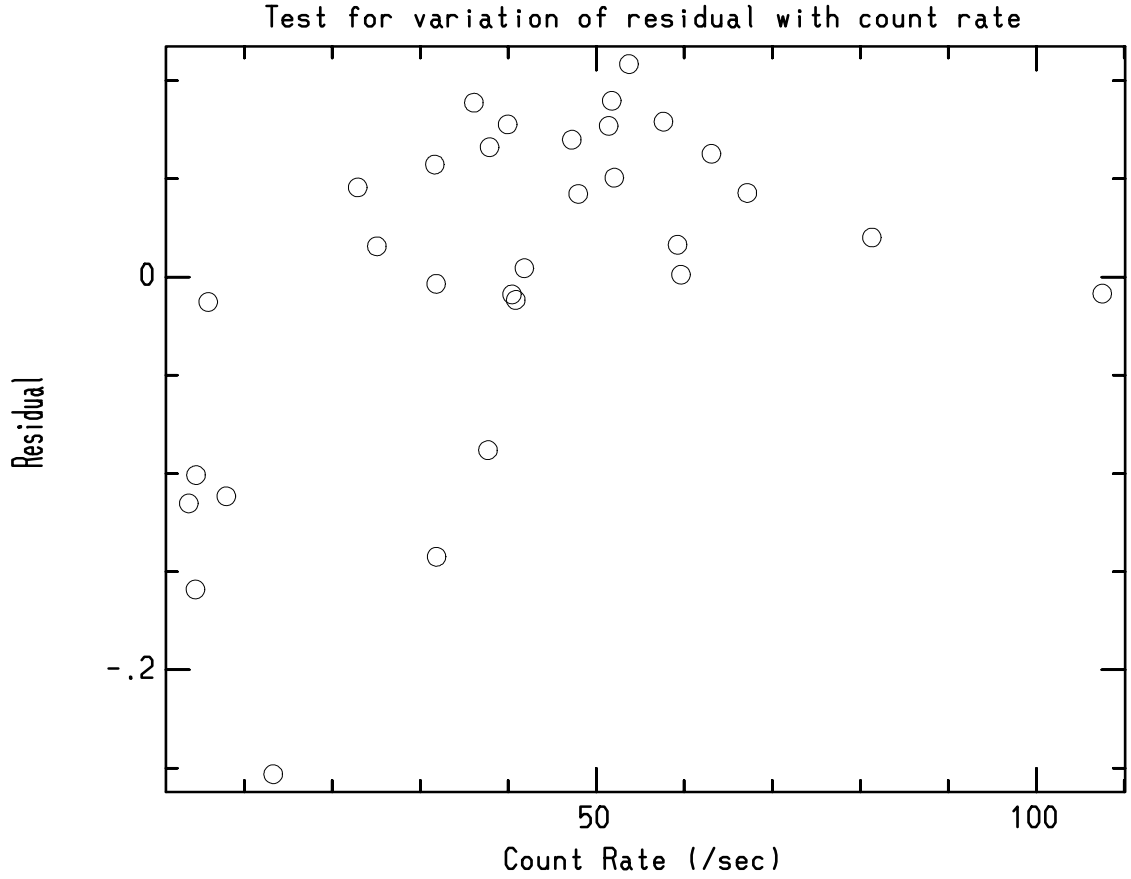

The expected nonlinearity for the ‘worst case’ image (HZ4 with F152M filter, with a total

count measured count rate of 108 counts/sec) was calculated using the methods outlined by Greenfield in FOC-ISR 074 (January 1994). The raw image, x2ap010ct.d0h, was convolved with a circular disk with radius 5.5 pixels and unit total counts. The resultant image was then corrected for nonlinearity using the **fflincorr** task in the **stsdas.hst_calib.foc.focphot** package using the default non-linearity parameter a=2.93 as appropriate for 256x256 F/96 normal format. The uncorrected smoothed image was then divided into the linearized image to give a map of nonlinearity (i.e. linearized flux/nonlinear flux) for each pixel. This map was then multiplied by the raw .d0h data, and the resulting image pipeline calibrated using the same reference files as the original data.

It was found that the measured encircled energy for the corrected image was about 6% higher than that for the uncorrected image. This was considered a small enough correction for even the most severely nonlinear data in the sample that it could be ignored.

This leaves 25 observations from the original sample of 44, and the r.m.s. residual is reduced to 0.055. The plot of the ratio of observed/expected against wavelength for the points that survived the weeding process is presented in Figure 3 below.

Figure 3: Final plot of observed/expected vs. wavelength for those observations that survived the weeding process

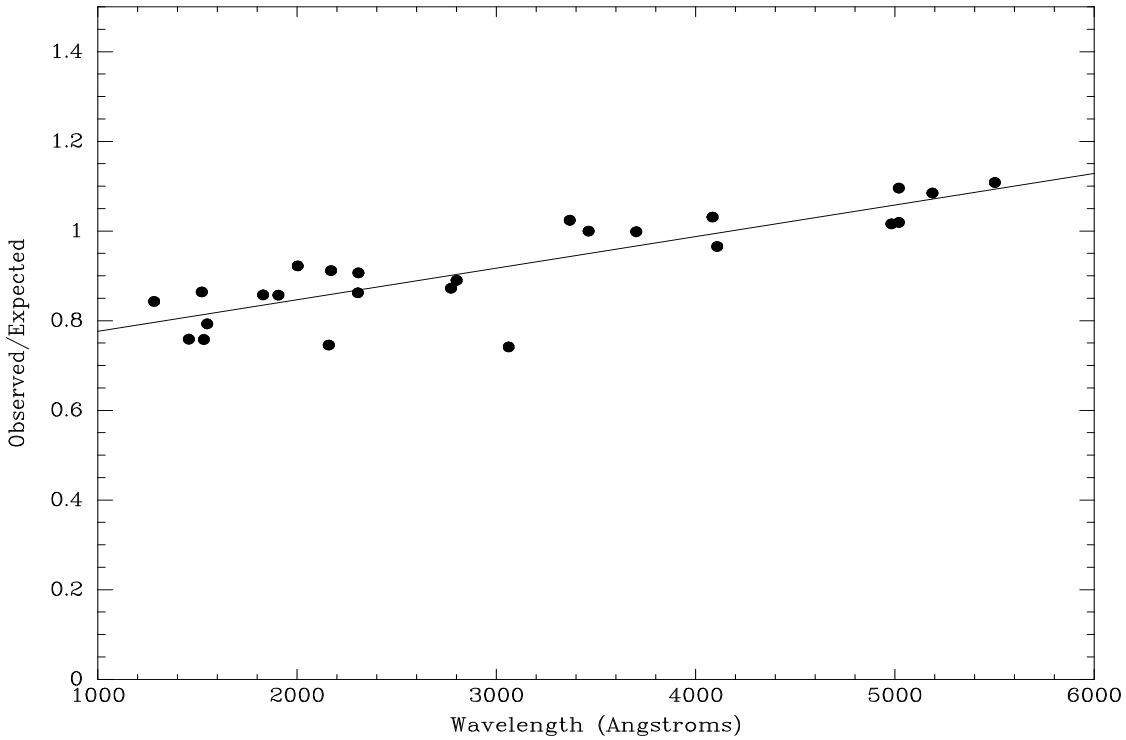

The r.m.s. residual for these points is an impressive 0.0553. The two points that have a significantly low value for the (Observed/Expected) ratio are the F307M+F4ND observation of BPM16274 (residual = -0.179) and the F210M+F2ND observation of HZ4 (residual =

-0.112). All other residuals are below 0.1.

5. Installation into the Routine Science Data Pipeline

The straight-line fit derived from these data is:

$$\frac{\text{Observed}}{\text{Expected}} = 1.0 + 0.342\left(\frac{\lambda}{4675} - 1\right)$$

where λ is measured in Angstroms. To correct the FOC DQE curve, the THROUGHPUT element of the curve was multiplied by this linear relation to give a corrected throughput curve (foc_96_dqe_004). The predicted count rate for each observation was then re-calculated with the corrected throughput curve. The resultant distribution is shown in Figure 4.

Figure 4: Ratio of observed to expected counts after re-calculation of **synphot** prediction using the new FOC DQE file. The straight line is a least-squares fit to the data points.

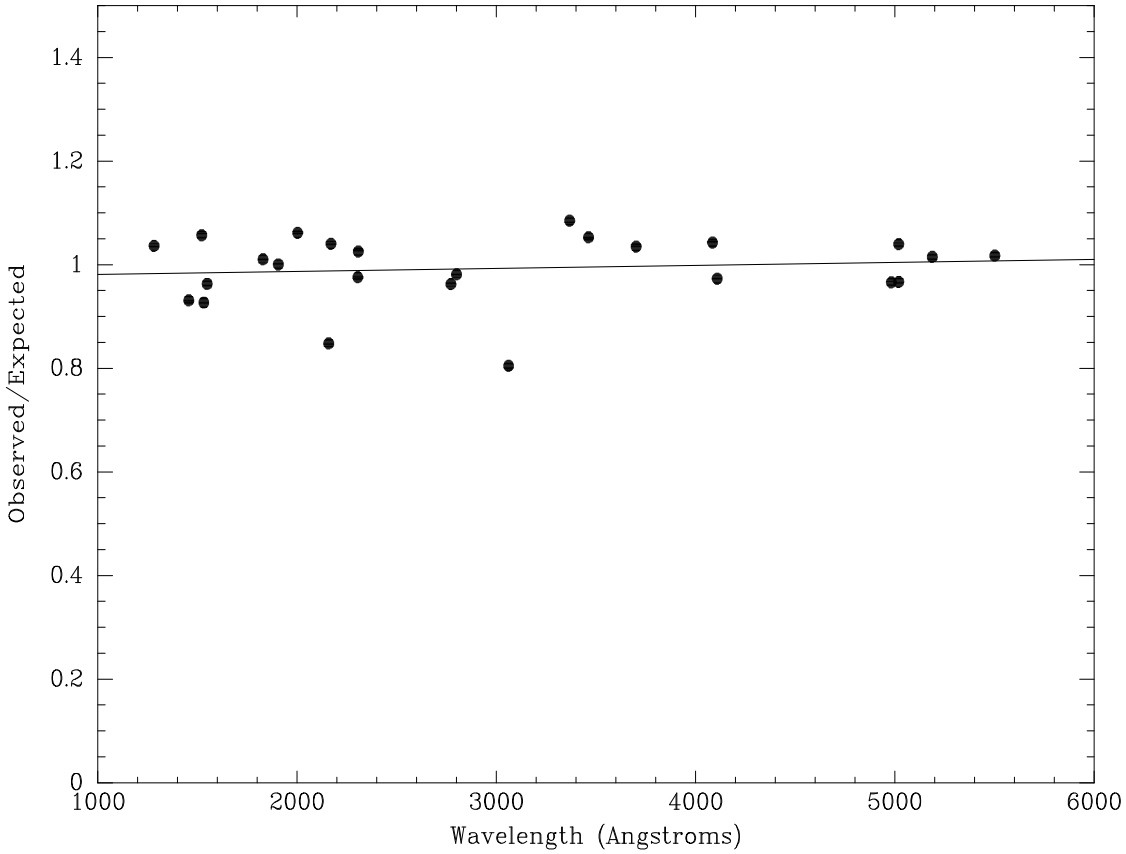

It can be seen that the points are not quite distributed evenly about a horizontal line with value 1.0, although the difference is small. A straight-line fit of the points gives 0.98 at 1000Å and 1.01 at 6000Å, with an r.m.s. residual of 0.064. The error on the slope is approximately twice its amplitude.

The r.m.s residual states that the 1σ error on a single measurement is approximately 6% (assuming that the IUE and visible flux measurements are perfectly accurate). In reality, the scatter of the measured points is probably significantly greater than any error in the reference spectrophotometry, so it is reasonably accurate to say that FOC observations can be placed on an absolute scale at the 6% accuracy level.

It should be noted that most of the fitted points (20 out of 25) are from HZ4, so our absolute calibrations are somewhat tied to that particular standard. Where the 5 observations of BPM16274 overlap with the HZ4 measurements, there is very good agreement, which gives confidence that the reference measurements are reliable. Calibration observations in the next Cycle will address this by using a different standard.

The new DQE curve (foc_96_dqe_004.tab) was installed into the HST pipeline on 18th October 1994. Users can check whether their observations used the new DQE curve by looking at the HISTORY records of the .c1h file. Using the IRAF command

```
cl> match dqe filename.c1h
```

should give a result like this:

```
HISTORY crfoccomp$foc_96_n256_001.tab, crfoccomp$foc_96_dqe_003.tab
```

where it can be seen that the OLD dqe curve was in use. Users can calculate the correct inverse sensitivity (PHOTFLAM keyword) for their data using **synphot** with the correct DQE curve (crfoccomp$foc_96_dqe_004.tab) using the following command in the **synphot** package:

```
sy> calcphot obsmode=band(PHOTMODE) spectrum='unit(flam,1.0)'
```

where the value of the PHOTMODE keyword derived from the .c1h file is substituted into the first bracket (e.g. foc, f/96,costar,f342w,x96n256 for a post-COSTAR F342W image in the 256x256 format). The value of PHOTFLAM is then given by 1.0/(calcphot.result).

Users can determine the FOC DQE file in use by their synphot installation by doing:

```
sy> grafpath "foc,f/96,costar" | match dqe
```

which should give the result:

```
crfoccomp$foc_96_dqe_004.tab
```

when the new DQE file is in place.

6. Check on ND filter transmissions

Since almost all of the observations use Neutral Density (ND) filters, it is worthwhile checking whether these filters are behaving in the way they are supposed to. This was prompted by analysis of INTFLATs with and without NDs that showed a significant difference between the flux ratios with and without the ND filters. Of course one cannot get a meaningful measurement of the flux for a target both with and without the F8ND filter, for example, since the observation with filter will generally be lost in the noise while that without will be saturated, since the flux difference will be a factor of 1000 or so. However,

it is possible to check whether all the observations that use a certain ND filter show any systematic difference in terms of (Observed/Expected) ratio when compared to all the observations that don't use that filter. Only the 25 observations that survived the weeding process were considered. It must be remembered that almost all of the observations use at least 1 ND filter, so this type of comparison will not be able to determine the absolute throughputs of the ND filters, just the values relative to each other. For example, if each ND filter were 10% lower than the CDBS values, such a comparison would probably not detect any difference between observations taken with one set of NDs with other observations that use a different set.

F1ND

10 out of 25 observations use the F1ND filter. The mean value for the (Observed/Expected) ratio was found to be 1.010 for those 10 observations, and 0.981 for the 15 observations that do not use the F1ND filter. The error on these means is 0.013, so the difference of 0.029 is significant at only the 2σ level.

F2ND

10 out of 25 observations use the F2ND filter. The mean value for the (Observed/Expected) ratio was found to be 0.9837 for those 10 observations, and 0.9983 for the 15 observations that do not use the F2ND filter. The error on these means is again 0.013, so here the difference of 0.0146 is only significant at only the 1σ level.

F4ND

Again, 10 out of 25 observations use the F4ND filter. The mean value for the (Observed/Expected) ratio was found to be 0.9953 for those 10 observations, and 0.9906 for the 15 observations that do not use the F4ND filter. The error on these means is 0.013, so the difference of 0.0047 is completely insignificant.

Overall, there appears to be no evidence for any systematic deviation of the throughputs of the neutral density filters on the basis of the observations that survived the weeding process. However, there might have been a subtle bias that influenced the observations that were weeded out, in that observations including a certain ND filter were selectively removed. Further work is needed to verify the accuracy of the ND filter transmissions.

7. Performance

Having measured the absolute sensitivity of the FOC and obtained PSF images for many of the most used filters, it is worthwhile to try and put the performance of the FOC as an imager into context by giving some performance measurements that are useful in determining the suitability of the FOC for certain observations.

Pseudo-Strehl Ratio

Using **synphot** with the new DQE curve will allow one to calculate the total count rate expected from a star with a certain flux. However, this does not fully convey what one might expect to see in an image, since there is no knowledge of the PSF. The most important specification of the PSF performance is the so-called “Pseudo-Strehl” ratio, defined as the ratio of the flux in the central pixel to the total flux. The larger this fraction, the “better” the observations will be. This is obviously determined by the pixel size, optical aberrations and the wavelength.

The Pseudo-Strehl ratio was measured for the observations used in this analysis by simply dividing the pixel intensity in the peak of the PSF in the .d0h file (so as to avoid resampling degradation) by the total intensity measured in the .c1h file. This is plotted against wavelength in Figure 5.

Figure 5: Plot of Pseudo-Strehl ratio for the PSF images examined here.

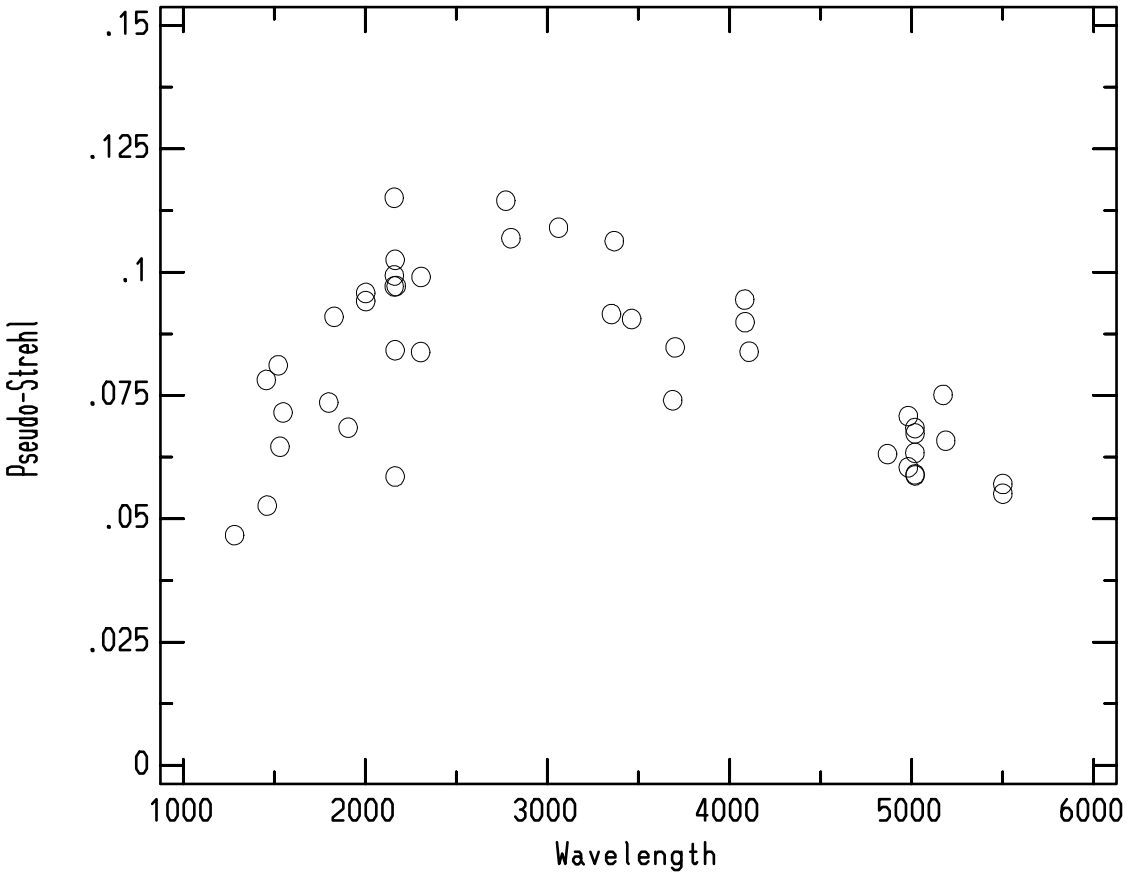

It can be seen that for the wavelength range between 2000Å and 3500Å that 10% of the flux of the PSF is contained within the central pixel. Longer than this, diffraction effects become significant while shorter than this, the small-scale aberrations scatter flux out of the central pixel into neighboring ones. Still, this performance is virtually diffraction-lim-

ited for wavelengths longer than 3000Å. It should be pointed out that before COSTAR corrected the spherical aberration, the Pseudo-Strehl values were typically 0.5-1.5%!

UV sensitivity

It is instructive to compare the UV sensitivity with that of WFPC2. To do this, the count rates were calculated for a 10^{-16} erg/cm^2/s/Å source through the wide-band FOC and WFPC2 filters. The results are presented in Figure 6. It can be seen that the FOC sensitivity is significantly greater than that of WFPC2 for all wavelengths below 4500 Å, by a factor of 2-4. The crossover point, where the sensitivities are approximately equal, occurs at the B-band (F430W for FOC, F439W for WFPC2).

Figure 6: Comparison of FOC and WFPC2 UV sensitivities.The plotted symbol identifies the filter, with the WFPC2 filters in **bold**.

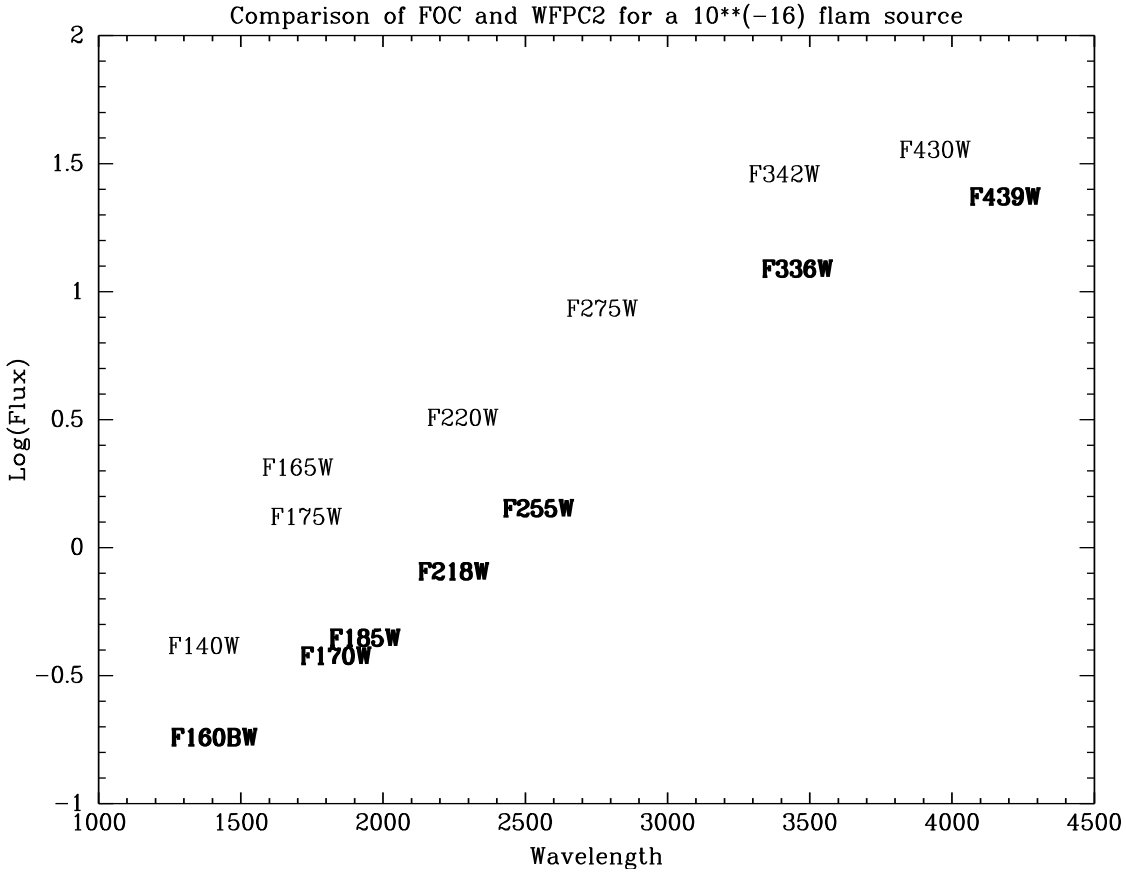

FWHM

The FWHM gives information on the detail that might be present in FOC images. It was measured by analyzing row and column plots of the raw (.d0h) data. Simple linear interpolation gave the position at which the intensity fell to one half of the peak value. No attempt was made to model the PSF to estimate the ‘true’ (i.e. infinitely well-sampled) peak inten-

sity, so the FWHM measurements are slightly biased to higher values.

The results of this analysis are shown in Figure 7. It can be seen that the FWHM is as low as 2 pixels for wavelengths below 3500Å, while the rise at longer wavelengths than this is due to diffraction. Note that one PC pixel is 0.045 pixels, so the FWHM is less than 1 PC pixel over the whole useful range of the FOC.

Figure 7: Plot of FWHM as a function of wavelength for F/96 PSFs

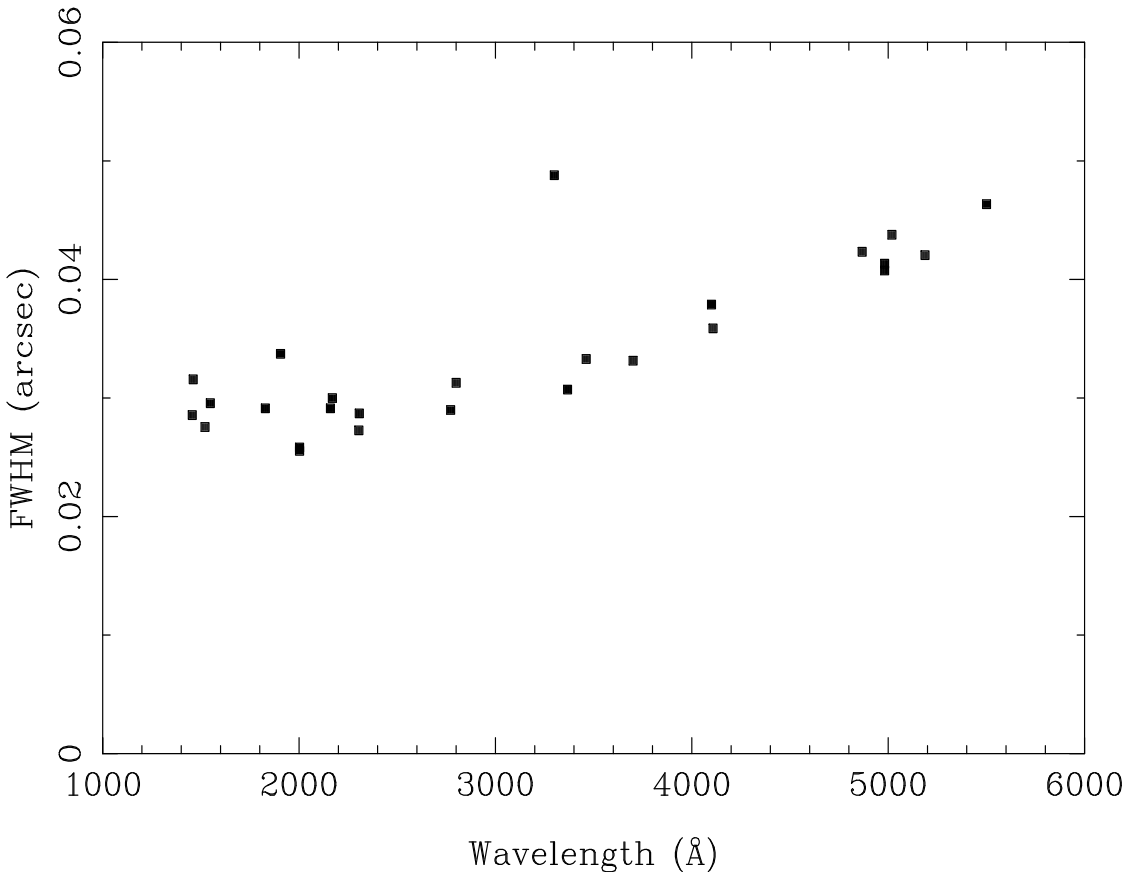

8. Summary

The absolute sensitivity of the FOC F/96 relay has been determined by comparing the measured fluxes of spectrophotometric standards with **synphot** predictions. Due to constraints on the field of view the normalization radius (within which all the flux is measured and where the background is defined) is smaller than for the pre-COSTAR case, leading to a significant apparent drop in sensitivity at UV wavelengths. A linear relation between (Observed/Expected) and wavelength was measured and applied to the absolute sensitivity curve of the FOC. The r.m.s. error of a single absolute flux measurement is 6.5% after correction.

The throughputs of the ND filters were checked and found to show no evidence for devia-

tion from the CDBS values, although more work is needed. Finally, the performance of the FOC was put into a context that will allow users to determine whether the FOC would provide a useful imaging tool for their science.